J. Micromech. Microeng. **19** (2009) 022001 (5pp) doi:10.1088/0960-1317/19/2/022001

BRIEF COMMUNICATION

Piezoelectric ultrasonic resonant motor with stator diameter less than 250 μm: the *Proteus* motor

B Watson, J Friend and L Yeo

Micro/Nanophysics Laboratory, Department of Mechanical and Aerospace Eningeering, Monash University, Wellington Road, Clayton, VIC 3800, Australia

E-mail: james.friend@eng.monash.edu.au

Received 25 September 2008, in final form 18 November 2008
Published 20 January 2009
Online at stacks.iop.org/JMM/19/022001

Abstract
Minimally invasive and *in vivo* surgery is limited by the ability to provide controllable and powerful motion at scales appropriate for navigation within the human body. A motor for *in vivo* microbot propulsion is presented with a stator diameter of ϕ250 μm, demonstrating the potential to directly drive a flagellum for swimming at up to 1295 rpm with a torque of 13 nN m. The motor uses coupled axial-torsional vibration at 652–682 kHz in a helically cut structure excited by a thickness-polarized piezoelectric element. The output power is 4.25 μW, on the order of what is necessary to navigate small human arteries.

(Some figures in this article are in colour only in the electronic version)

1. Introduction

Opportunities for micro-motors and micro-actuators abound in fields as diverse as bio-medicine, electronics, aeronautics and the automotive industry. Responses to this need have been just as diverse, with designs developed using electromagnetic [1], electrostatic [2], thermal [3] and osmotic [4] driving forces. This paper specifically focuses on the need for small scale motors for medical procedures. In many circumstances, techniques used in minimally invasive surgery are inferior to standard cut and sew methods. Even the most complex minimally invasive surgical equipment reduces a surgeon's dexterity, feel and visibility [5]. To improve this, research is being carried out on systems that will permit procedures to be conducted on the micro-scale using remotely operated micro-robots (microbots). To facilitate this, micro-scale motors are required. A design that has significant potential in this area is one that uses ultrasonic vibrations driven by the converse piezoelectric effect. Piezoelectric ultrasonic actuators are familiar at the macro scale, with many examples in commercial products such as watches and cameras. These designs have favourable scaling characteristics [6] and, in general, are simple designs, which provide an excellent platform for the development of micro-motors and micro-actuators.

Piezoelectric ultrasonic motors with stator dimensions of approximately 1 mm and overall dimensions of only a few millimetres exist [7, 8], and, even smaller, linear actuators have been developed that fit into a cube 400 μm on a side [9]. However, a practical rotational actuator with dimensions significantly below 1 mm—a true *micro*-motor—has not yet been achieved. Here we detail the principle of operation, design, fabrication and initial results for a piezoelectric ultrasonic motor with a stator diameter of less than 250 μm. This stator design is approximately 70% smaller than the smallest design produced so far [8], and is the first step towards the design of a practical micro-motor. The intended application of this motor is in propulsion of micro or so-called 'nanorobots' [10] for autonomous non-invasive observation and surgery within the human body, the reason for naming it the *Proteus* motor after the project name used in Isaac Asimov's prescient *Fantastic Voyage* [11].

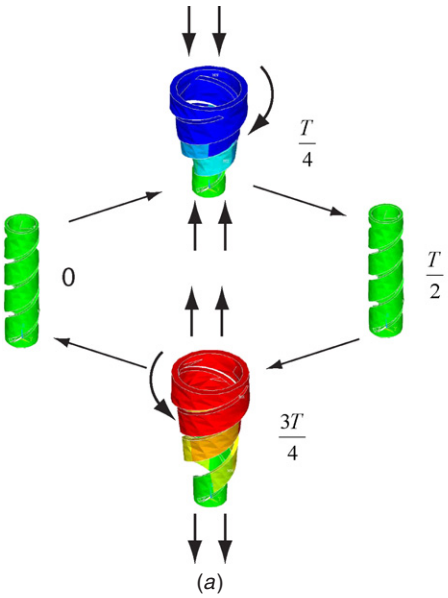

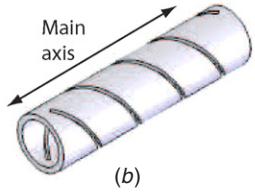

Object	Dimension (μm)
Base Tube	
Inside Diameter	200
Outside Diameter	241
Length	985
Helical Cut	
Width	28
Pitch	440
Length	880

(c)

Figure 1. Finite element analysis (*a*) confirmed the coupled axial and torsional motion of the helically cut stator (*b*) of dimensions significantly below 1 mm (*c*).

2. Basis of operation

Piezoelectric ultrasonic resonant micro-motors use the resonant vibration mode of the stator to amplify and control the induced strain of the piezoelectric element. By coupling resonant modes in the stator, an elliptical motion at the stator tip can be obtained. This elliptical motion can, through friction coupling, be converted to provide rotational motion [12]. The most successful and popular micro-motor designs to date use coupled orthogonal bending modes in the stator, driven through a spring-force friction coupling [7, 8]. These designs however, have fragile and difficult to fabricate piezoelectric stators. Moreover, complex stator designs and control systems provide obstacles to a further reduction in scale.

An alternative is to couple the axial and torsional modes of the stator. Such a design allows the coupled modes to be excited by one piezoelectric element not integral to the stator. This removes many of the obstacles associated with coupled bending mode designs. It is known that coupling axial and torsional modes can be achieved through geometric design, the most striking example of this being the Wilberforce pendulum [13]. However, limited research has been carried out to obtain practical stator designs, or to explore the potential design benefits at small scales, with only limited macro-scale designs having been developed [14, 15].

In response, we have developed a new stator design coupling torsional and axial displacements. The design uses a helical geometry machined with laser micro-machining technology (Norman Noble Inc., Highland Heights, OH, USA) to induce torsional motion during axial vibration, with a resulting motion reminiscent of a helical spring under axial loading. Due to a phase shift in the torsional response with respect to the axial motion, an elliptical motion of the stator tip is developed. This allows a net motion to be achieved through the friction coupling.

3. Design and fabrication

The finite element analysis program ANSYS V10.0 (ANSYS Inc., Canonsburg, PA, USA) was used to conduct an initial limited parametric study on the helical geometries. It modelled all stator geometries and used free boundary conditions at both ends. Through modal analysis, this study was used to qualitatively confirm the expected stator motion and to determine a robust, but not optimized, geometric design for fabrication. The stator motion is illustrated in figure 1. Future work will see the model expanded to include the piezoelectric element, which will allow an accurate comparison to experimental results and a model validation.

The fabricated design consists of a 304 stainless-steel tube, with two diametrically opposite helical cuts through the tube wall (fabricated by Norman Noble Inc., Highland Heights) also detailed in figure 1. The resonant modes are excited by a hard composition lead zirconate titanate (PZT) piezoelectric element (C203, Fuji Ceramics, Tokyo, Japan), bonded by epoxy to one end of the helically cut stator. The PZT element is 3.5 mm in length, 2.5 mm in width and 0.27 mm in thickness; thickness poled, and was chosen due to availability. The frequency of operation was well below any frequency that would excite an out-of-plane mode in the PZT. Therefore, as the thickness dimension (0.27 mm) is smaller than what one would expect to use in a finalized micro-motor (of PZT dimensions 0.25 mm × 0.25 mm × 0.5 mm thickness for example) the large element does not artificially improve the motor performance. Moreover, if we consider that a PZT element of 0.5 mm thickness can produce a larger displacement and accept a higher input voltage, both of which improve performance, the use of the larger element may reduce the motor performance. A conductive copper tape was used to attach the PZT/stator component to an alumina base for testing. All wiring was hand soldered. The friction coupling

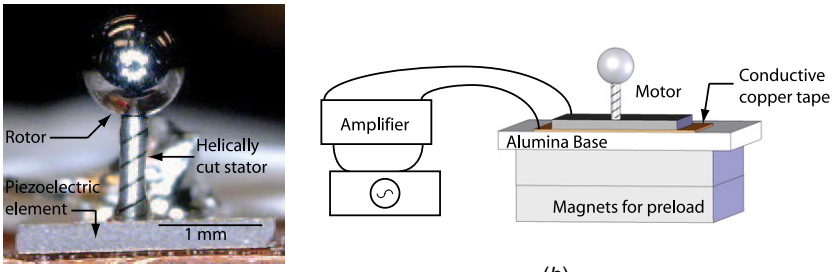

Figure 2. (*a*) Photo of the micro-motor prototype showing the $\phi 241$ μm helically cut stator, 1 mm stainless-steel ball as a rotor and the PZT element. (*b*) Magnets were used to increase the friction coupling preload.

was enhanced using a magnetic force acting on a hardened steel ball 1 mm in diameter (the rotor), to provide a preload of 39 μN. The steel ball was chosen to act as a rotor as it provided a clean reflective surface that assisted in the performance measurement, was easy to mount, had a homogeneous and predictable density, accepted a magnetic preload and provided a smooth consistent surface for operation. The test prototype can be seen in figure 2.

4. Method

A scanning laser Doppler vibrometer (LDV) and associated software (MSA–400, Polytec GmbH, Waldbronn, Germany) was used to measure motion along the thickness axis for the PZT element. Whilst simultaneously exciting all frequencies in the band 0–2 MHz, an axial displacement response spectrum was recorded. This response was compared with the response spectrum of the axial motion along the main axis of the stator (see figure 1). The stator spectrum was determined using the same method, and the same frequency band as for the PZT. Peaks in the axial motion of the stator tip, without the associated peaks in the PZT motion, were determined to be stator resonant modes. Each resonant mode was further analysed using the scanning LDV to classify the mode shape based on the displacement of the stator tip. Figure 3 shows the typical displacement profile of the stator tip for nominal axial and bending derived modes. The motor was designed to place the bending modes away from the axial and torsional modes of the motor. Rotor motion was recorded using a digital high speed camera (Olympus i-speed, Olympus Australia, Mount Waverley, Australia) at 1000 frames per second. The angular velocity versus time curve was determined using the Olympus i-speed image processing software (V1.16, Olympus Industrial America, Orangeburg, NY, USA).

5. Results and discussion

Through experimental trials, the motor was found to have the highest start-up torque and rotational velocity when driven at the stator axial resonance with the largest amplitude, 677 kHz. Using the technique described in section 4, this mode was found to be predominantly a high-order axial/torsional coupled mode. However, due to a small misalignment during fabrication and the nonlinearity of the design, bending and

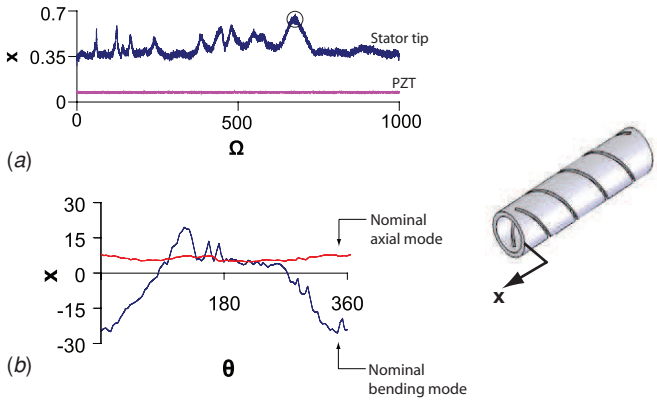

Figure 3. By comparing the axial response spectrum for the PZT and stator tip, the stator modes could be highlighted (*a*); x is the axial displacement in (nm) and Ω is the driving frequency (kHz). The circled area is the frequency of operation. These resonant frequencies were then analysed with the LDV to determine the mode shape (axial or bending based) (*b*): x is the axial displacement (nm) and θ is the circumferential position (degrees) around the free tip of the stator. Note an in-phase displacement amplitude over the whole tip for the axial mode, while the bending mode only has a positive displacement for approximately half of the circumference around the tip.

pinching modes were also weakly excited at this frequency. Further work will be required to determine the extent of the effect of these additions. Using a signal generator and amplifier (Rohde & Schwarz–SML 01 and NF–HSA 4501, North Ryde, NSW, Australia), the PZT element was driven at 677 kHz with an applied voltage 28.1 $V_{p–p}$, as measured with an oscilloscope (LeCroy WaveJet 334, Chestnut Ridge, NY, USA). The voltage was applied as a step input, resulting in the angular velocity versus time curve shown in figure 4. The fitted exponential curve is derived from the standard curve for a piezoelectric ultrasonic motor [16].

The maximum angular velocity recorded for the motor was 135 rad s^{-1} (1295 rpm). Using this as an input for the method developed by Nakamura *et al* [16] the maximum start-up torque, based on the curve shown in figure 4, was calculated to be 13 nNm. For the chosen operating mode, the motor had an operating frequency range of 652–682 kHz. Although performance varies across this range, having a large operational frequency band will allow flexibility in future applications for the motor, should frequency stabilization or modulation be important in power supplies. The performance

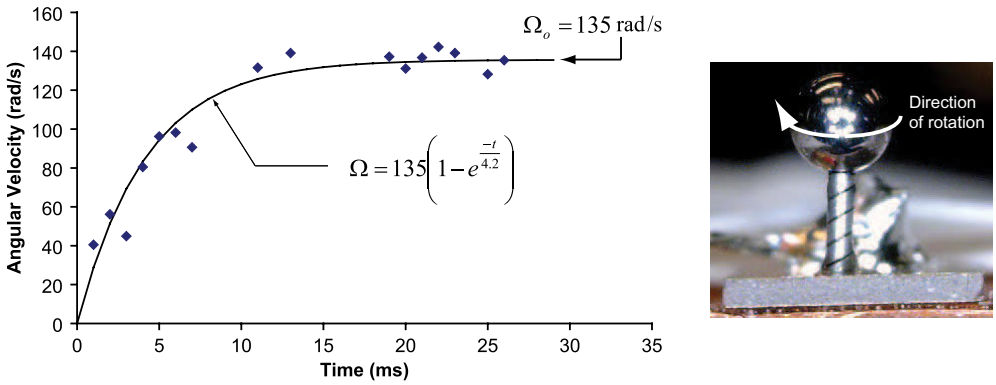

Figure 4. Angular velocity versus time results for an applied step voltage of 28.1 V_{p-p}, preload of 39 μN and a operating frequency of 677 kHz. The fitted curve is derived using the method outlined in [16].

of this new design compares well with other piezoelectric ultrasonic micro-motors; this design offers 52% of the torque with a stator 32% of the size of the most comparably sized device by Kanda *et al* [8].

To improve the motor performance, further work to match the torsional and axial resonance frequencies of the laser machined tubing with the thickness resonance of the piezoelectric element is to be carried out. To ensure this performance improvement is sustained whilst having a complete motor volume of less than 1 mm^3, it will be necessary to provide a new rotor arrangement that removes the need for large magnets currently used to provide a preload. This may ultimately be achieved through a mechanical 'snap-fit', however current research is focussed on a novel approach to casting magnetic components. As magnetic force is proportional to distance to the power of 4 ($F_{mag} \propto d^4$), it is hypothesised that a magnetic rotor will alleviate the need for the large magnets, or at the very least reduce the size required to within the desired volume range.

We now consider an application for the motor, that of the drive system for an *in vivo* 'swimming microbot' that uses an *E. coli*-like flagellum as a means of propulsion. Such microbots have been highlighted as having great potential for use in *in vivo* medical procedures due to the low Reynolds number propulsion system [17]. The power output of the reported motor is approximately $\phi_{max} T_{max}/4 = (135)(13 \times 10^{-9})/4\text{W} = 4.25\ \mu\text{W}$. Using Higdon's model for flagellar propulsion [18], we may determine the average power required for swimming in small human arteries from $\bar{P} = 6\pi\mu A\bar{U}^2\eta_0^{-1}K$; blood has a viscosity of approximately $\mu = 0.0035$ Pa s [19], A is the radius of the swimming microbot which we will assume to be approximately the size of the motor, 150 μm, and K is Stokes' law correction for a prolate spheroid, 2.7 [20]. From Higdon's results, we take $\eta_0^{-1} = 200$, which leaves only the swimming speed $\bar{U}$ to be defined. If we presume the device should at least swim as fast as the blood flow, and consider the right central retinal artery as a suitable example of a location both difficult to reach by other means and one where this device would be used, $\bar{U} \approx 6.0$ cm s^{-1} [21], giving 19 μW of power. This demonstrates that potentially the motor could propel such a microbot.

6. Conclusions

We have demonstrated a piezoelectric ultrasonic resonant motor that uses coupled axial and torsional displacements, derived from a helically cut stator. This novel stator design enables us to overcome many of the problems associated with current designs and produce a stator that is less fragile, simpler to control and more than 70% smaller than the smallest stator design produced thus far. With further research, such motor designs potentially open the door to new areas of *in vivo* surgery and micro-robotics.

Acknowledgments

This work was made possible in part by grants SM/07/1616 and SM/06/1208 from the CASS Foundation, grant DP0773221 from the Australian Research Council, and the New Staff and Small Grant Scheme funds from Monash University.

References

[1] Hori K, Miyagawa T and Ito K 1997 Development of ultra-small sized servo actuator with brushless DC motor, planetary gear drive and optical rotary encoder *Int. J. Japan Soc. Precis. Eng.* **31** 1–5
[2] Mehregany M, Nagarkar P, Senturia S D and Lang J H 1990 Operation of microfabricated harmonic and ordinary side-drive motors *Proc. IEEE Micro-Electro-Mechanical Systems Workshop* p 8
[3] Sinclair M J 2000 A high force low area MEMS thermal actuator *Seventh Intersociety Conf. on Thermal and Thermomechanical Phenomena in Electronic Systems*
[4] Su Y-C, Lin L and Pisano A P 2002 A water-powered osmotic microactuator *J. Microelectromech. Syst.* **11** 736–42
[5] Hanly E and Talamini M 2004 Robotic abdominal surgery *Am. J. Surg.* **188** 19S–26
[6] Wang Z L 2007 Nanopiezotronics *Adv. Mater.* **19** 889–92
[7] Morita T, Kurosawa M K and Higuchi T 2000 A cylindrical shaped micro ultrasonic motor utilizing PZT thin film 1.4 mm in diameter and 5.0 mm long stator transducer *Sensors Actuators* **83** 225–30
[8] Kanda T, Makino A, Suzumori K, Morita T and Kurosawa M K 2004 A cylindrical micro ultrasonic motor

using a micro-machined bulk piezoelectric transducer *IEEE Ultrasonics Symp.*

[9] Friend J, Yeo L and Hogg M 2008 Piezoelectric ultrasonic bidirectional linear actuator for micropositioning fulfilling Feynman's criteria *Appl. Phys. Lett.* **92** 014107

[10] Sitti M 2001 Survey of nanomanipulation systems *IEEE-NANO 2001: Proc. 2001 1st IEEE Conf. on Nanotechnology* pp 75–80

[11] Asimov I 1966 *Fantastic Voyage: A Novel* (Boston: Houghton Mifflin)

[12] Uchino K 1998 Piezoelectric ultrasonic motors: overview *Smart Mater. Struct.* **7** 13

[13] Berg R E and Marshall T S 1991 Wilberforce pendulum oscillations and normal modes *Am. J. Phys.* **59** 32–8

[14] Wajchman D, Liu D, Friend J and Yeo L 2008 An ultrasonic piezoelectric motor utilising a non-circular cross-sectioned twisted beam *IEEE Trans. Ultrason. Ferroelectr. Freq. Control* **55** 832–40

[15] Tsujino J 1998 Ultrasonic motor using a one-dimensional longitudinal-torsional vibration converter with diagonal slits *Smart Mater. Struct.* **7** 345–51

[16] Nakamura K, Kurosawa M, Kurebayashi H and Ueha S 1991 An estimation of load characteristics of an ultrasonic motor by measuring transient responses *IEEE Trans. Ultrason. Ferroelectr. Freq. Control* **38** 481–5

[17] Behkam B and Sitti M 2006 Design methodology for biomimetic propulsion of miniature swimming robots *ASME J. Dynamic Syst. Meas. Control* **128** 36–43

[18] Higdon J J L 1978 The hydrodynamics of flagellar propulsion: helical waves *J. Fluid Mechanics* **94** 331–51

[19] Rand P W, Lacombe E, Hunt H E and Austin W H 1964 Viscosity of normal human blood under normothermic and hypothermic conditions *J. Appl. Physiol.* **19** 117–22

[20] Happel J and Brenner H 1965 *Low Reynolds Number Hydrodynamics* (Englewood Cliffs, NJ: Prentice Hall)

[21] Fuchsjger-Mayrl G, Polak K, Luksch A, Polska E, Dorner G T, Rainer G, Eichler H-G and Schmetterer L 2001 Retinal blood flow and systemic blood pressure in healthy young subjects *Graefes Arch. Clin. Exp. Ophthalmol.* **239** 673–7